

High-speed axial-scanning wide-field microscopy for volumetric particle tracking velocimetry

T.-H. Chen¹ · J. T. Ault¹ · H. A. Stone¹ · C. B. Arnold¹

Received: 28 April 2016 / Revised: 20 January 2017 / Accepted: 10 February 2017 / Published online: 3 April 2017
© Springer-Verlag Berlin Heidelberg 2017

Abstract The ability to understand and visualize complex flow structures in microfluidic and biological systems relies heavily on the resolving power of three-dimensional (3D) particle velocimetry techniques. We propose a simple technique for acquiring volumetric particle information with the potential for microsecond time resolution. By utilizing a fast varifocal lens in a modified wide-field microscope, we capture both volumetric and planar information with microsecond time resolution. The technique is demonstrated by tracking particle motions in the complex, three-dimensional flow in a high Reynolds number laminar flow at a branching arrow-shaped junction.

1 Introduction

Micron-scale volumetric velocimetry measurements are invaluable to understanding many of the complex flow structures found throughout the fields of fluid dynamics, engineering, and life sciences (Westerweel et al. 2013; Choi and Lee 2009; Dennis and Nickels 2011; Wereley and

Meinhart 2010; Vigolo et al. 2014). The ability of three-dimensional (3D) velocimetry techniques to accurately track particles relies on the resolving power of 3D imaging techniques (Klein et al. 2012; Cierpka and Kähler 2011). Retrieving out-of-plane motions has been the major challenge of 3D imaging techniques and has attracted a significant interest in the recent literature. One common method to obtain information along a third axis is to set up multiple cameras, as is done in tomographic and stereographic imaging (Elsinga et al. 2006; Prasad 2000). However, setting up multiple optical paths not only increases the complexity of the system and difficulty in reconstructing the data, but it also increases the cost of the system. Another strategy to obtain out-of-plane motions without using multiple cameras is to acquire planar information at different positions on the optical axis. This is sometimes done by utilizing optical effects of the tracked object, moving the linear stage, and/or using varifocal optics (Park and Kihm 2005; Pereira and Gharib 2002; Grothe and Dabiri 2008; Willert and Gharib 1992; Zong et al. 2014; Mermillod-Blondin et al. 2008; Chen et al. 2014; Park et al. 2004; Olivier et al. 2009; Duocastella et al. 2014; Vettenburg et al. 2014).

Several optical effects that can be used to reconstruct out-of-plane motions of tracked objects have been proposed (Park and Kihm 2005; Pereira and Gharib 2002; Grothe and Dabiri 2008; Willert and Gharib 1992). However, insufficient imaging depth has been a major limitation of these techniques. Other methods, such as utilizing a linear stage or varifocal optics, provide sufficient and flexible imaging depth. However, these step-wise approaches suffer from limitations in image acquisition due to the scanning speed of the stage or the varifocal optics (Chen et al. 2014; Park et al. 2004; Vettenburg et al. 2014). Among the varifocal optics, tunable acoustic gradient index (TAG) lenses provide the

NSF (Grant No. CMMI-1235291) and the Ministry of Education, Republic of China.

✉ C. B. Arnold
cbarnold@princeton.edu

T.-H. Chen
tc6@princeton.edu

J. T. Ault
ault@princeton.edu

H. A. Stone
hastone@princeton.edu

¹ Department of Mechanical and Aerospace Engineering, Princeton University, Princeton, NJ 08544, USA

highest scanning frequency, ranging from 50 kHz to 1 MHz. TAG lenses have been used along with various imaging setups including confocal microscopy, two-photon microscopy, and light-sheet microscopy (Zong et al. 2014; Mermillod-Blondin et al. 2008; Olivier et al. 2009; Duocastella et al. 2014). With confocal and two-photon microscopy, planar information is derived by point scanning, which lowers the image acquisition rate. Here, we present a simple and fast 3D imaging technique by integrating wide-field microscopy with a TAG lens to perform volumetric velocimetry measurements.

The unique imaging capabilities of our approach are enabled by the fast axial scanning of a TAG lens. TAG lenses consist of a fluid-filled cylindrical cavity in which a piezo material is excited to form an acoustic wave within the fluid, creating periodic variations of the refractive index (McLeod and Arnold 2007; Duocastella et al. 2012). The refractive index of the lens has been shown to be a Bessel function in space and a sinusoidal function in time. As a result, the focal length of the optical system oscillates as a sinusoidal function at the driving frequency. To capture images at different focal lengths, we trigger an LED light source and the camera shutter simultaneously at a delayed time. An image frame is then captured at a certain phase of the sinusoidal function of the focal length. Hence, we are able to obtain images at different focal planes by altering the delay time to trigger the LED and camera shutter. Thus, this method not only allows one to select the number and position of each focal plane of interest, but also allows selection of the temporal and spatial resolution of the velocimetry technique in general.

2 Materials and methods

2.1 Imaging system

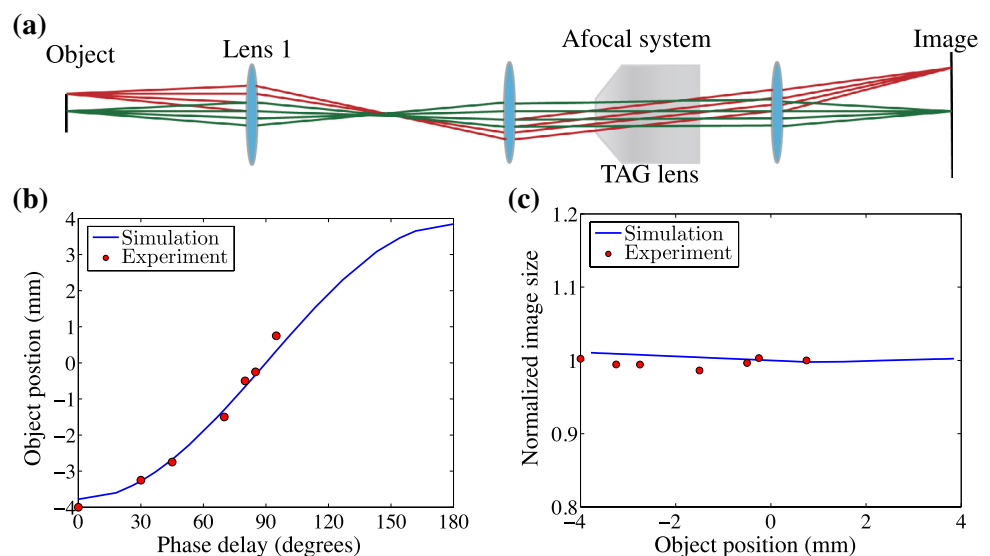
The main idea of this imaging technique is to acquire stacks of 2D images by varying the positions of the focal plane with the TAG lens. However, without proper compensation, the image size will scale with the object's position. This change of magnification will then reduce the accuracy of volumetric information. Constant magnification can be achieved by placing the principal plane of the tunable optics at the aperture stop of the objective lens. This step could be verified by geometric optics. However, the aperture stop usually is not accessible, requiring an afocal system to transfer the aperture stop to an accessible position for the tunable optics. Such an arrangement is commonly called a "4f" system. To verify that an afocal system can be used in this way to obtain constant magnification, we simulate our afocal system with the TAG lens using Zemax (Zemax LLC). The layout of the system is shown in Fig. 1a.

Here, we simulate the TAG lens as a time-varying gradient index lens, whose refractive index n can be written as follows:

$$n = n_0 + n_A J_0 \left(\frac{\omega \rho}{c_s} \right) \cos(\omega t), \quad (1)$$

where n_0 is the static refractive index of the filling fluid, ω is the driving frequency, c_s is the speed of sound of the filling fluid, t is the phase delay, and ρ is the radial coordinate in the lens plane (McLeod and Arnold 2007). In addition, n_A is related to the driving power of the piezo-electric element, whose value is calibrated using experiments. By altering the phase delay, the refractive index and hence

Fig. 1 **a** Demonstration of simulation and experimental setup for integrating the afocal system and TAG lens. **b** Experimental focal plane positions compared with simulation results as a function of the phase delay. **c** Normalized image size as a function of the object's position (image sizes have been normalized by the image size at $z = 0$). Experimental results show good agreement with the simulation results. Experimental results here are highly reproducible, such that *error bars* will not be visible on these plots



the focal length of the system change correspondingly. We find that the principal plane of the TAG lens is shifted on the order of $1\ \mu\text{m}$ within the scanning range. However, the magnification error does not exceed 0.1% of the image size when the principal plane of the TAG lens is properly aligned with the aperture stop of the system. The experimental and simulation results are shown in Fig. 1b and c, demonstrating both the sinusoidal function of focal length and the constant magnification at different focal lengths.

We now incorporate the TAG lens and afocal relay system into a wide-field microscopy setup for particle tracking. A graphical representation of this imaging setup is shown in Fig. 2. The primary components of the imaging system are a pulsed high-power white LED, a Fluar 5x/0.25 objective lens (Carl Zeiss Microscopy, LLC), a TAG lens (Model TL25.β, TAG Optics Inc.), and a high-speed CMOS camera (Phantom v7.3, Vision Research).

2.2 Experimental flow systems

To test our imaging approach in a flow system, we begin with the simple case of a straight-square channel. In this case, we flow $45\ \mu\text{m}$ diameter (d_p) polystyrene beads

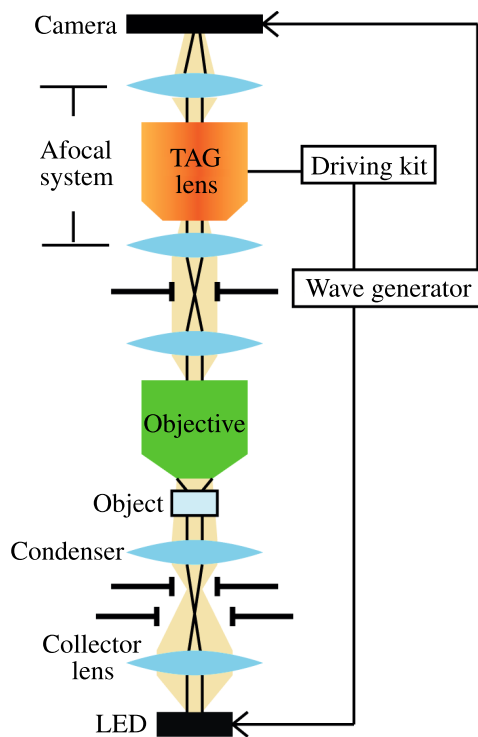


Fig. 2 Experimental setup. The illuminating ray paths are sketched as *yellow lines* and the image-forming ray paths are sketched as *black lines*. The driving kit sends RF signals to drive the TAG lens and wave generator simultaneously. The wave generator then sends out delayed transistor–transistor logic (TTL) pulses to trigger both the pulsed LED and camera shutter at the same time

through a $1\ \text{mm}$ by $1\ \text{mm}$ square channel in a 21% by weight glycerol solution. This mixture was selected to match the density of the particles and prevent rising or settling due to buoyancy effects. Here, the Stokes number $St = \rho_p d_p^2 U_{\text{avg}} / (18\mu\ell_w)$ is about 1.1×10^{-4} , and thus, the particles can be expected to track the fluid streamlines quite well. The fluid flows at a Reynolds number of $Re = \rho U_{\text{avg}} \ell_w / \mu = 1$. We apply a low seeding density ($\approx 2 \times 10^4\ \text{mL}^{-1}$) to avoid particle overlapping; however, higher densities can be used with more advanced particle tracking algorithms. This experimental setup will allow us to provide a quantitative comparison between the measured particle velocities in a simple 3D flow with theoretical predictions.

The desired application of this imaging setup is to accurately and quickly track particles in flows with complex 3D structures. Recent fluid dynamics research has revealed that the flows in simple T-, Y-, and arrow-shaped junctions have a complex 3D structure that can develop recirculation zones and even lead to unexpected particle trapping in some cases (Vigolo et al. 2014; Chen et al. 2015; Vigolo et al. 2013). Because of the 3D nature of these flows and the interesting particle behaviors that can arise in them, we also perform experiments in an arrow-shaped geometry with junction angle $\theta = 70^\circ$ (Fig. 3).

For these arrow-shaped experiments, we use a square channel with cross-sectional dimension $\ell_w = 800\ \mu\text{m}$. As in the prior literature, we use as our fluid a 0.2 M solution of sodium polytungstate, which has a density of $\rho = 1450\ \text{kg/m}^3$ and a viscosity of $1.5 \times 10^{-3}\ \text{Pa s}$ at a room temperature of 23.5°C (Ault et al. 2016). We use an average inlet velocity of $U_{\text{avg}} = 0.206\ \text{m/s}$, which gives a flow Reynolds number of $Re = \rho U_{\text{avg}} \ell_w / \mu = 160$. For this Reynolds number, we expect the flow to contain swirling 3D

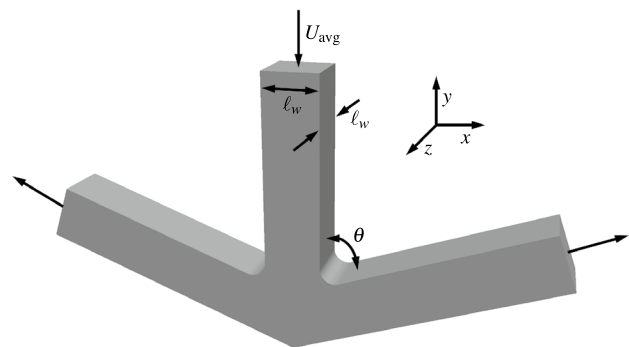


Fig. 3 Experimental geometry and numerical simulation domain. The flow enters through the *top* with average velocity U_{avg} and splits between the two outlets. The channel cross-section is *square* with dimension ℓ_w , and the *arrow-junction* turns through an angle θ . The directions of x , y , and z are shown on the figure. The origin is taken to be at the *bottom* vertex of the junction at a depth of half the channel height

vortical features in the junction that travel into the outlets and decay downstream. We add polystyrene beads with diameter $d_p = 45 \mu\text{m}$ to the flow. These particles have a density of $\rho_p = 1030 \text{ kg/m}^3$, giving a Stokes number of $St = \rho_p d_p^2 U_{\text{avg}} / (18 \mu \ell_w) = 0.02$. With this value, the particles can be expected to approximately follow the streamlines of the flow.

3 Results and discussion

3.1 Imaging capabilities

We first define the axial imaging volume. The ideal field size is D/M , where D is the size of the camera chip and M is the magnification of the system. The available imaging depth of the volume along the optical axis, Δz , can be written as a function of the objective properties and the optical power of the lens as previously reported (Duocastella et al. 2012). In our specific system, a $5\times$ objective (N.A. 0.25) is used in the wide-field microscope and the lens is driven at 25.6 V, yielding a field size of 2.5 mm and an maximum imaging depth of $600 \mu\text{m}$.

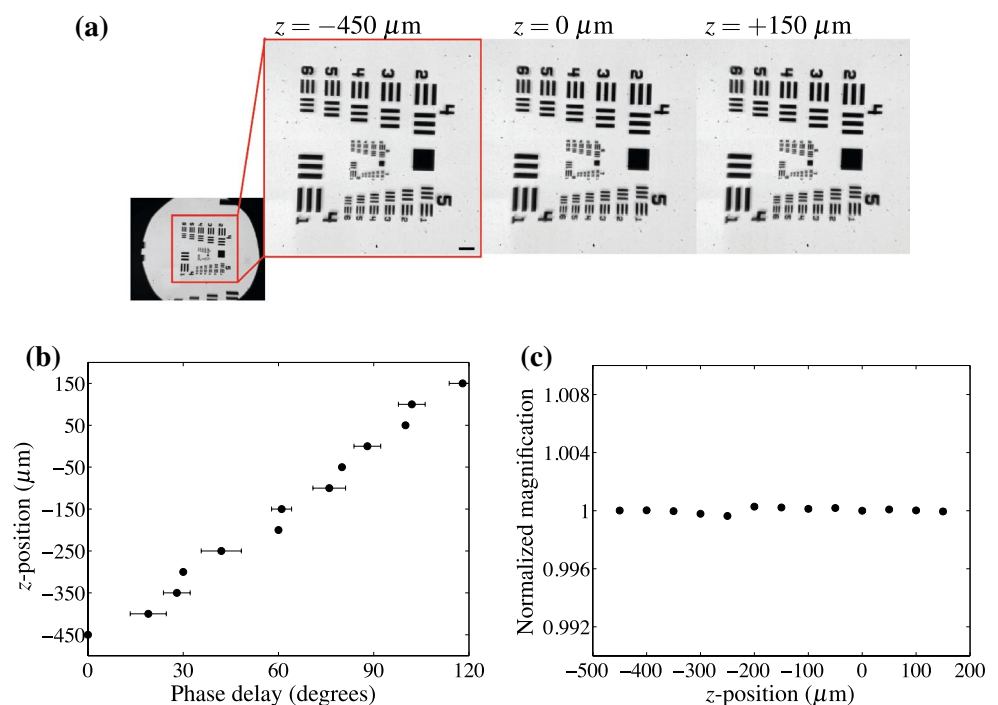
Compared to other varifocal devices, the high scanning frequency of a TAG lens allows the system to scan through the full axial imaging range at a much higher rate. By sending delayed pulses of light within one cycle of the TAG lens oscillation and synchronizing with the camera shutter, we can acquire as many image planes within our imaging volume as the camera frame rate allows. In our experiments

here, the TAG lens is driven at 70 kHz, which is the minimum resonance frequency for the system. Since we are limited by the frame rate of our high-speed camera, there is no benefit to drive the lens at a higher frequency. In Fig. 4a, each image is taken at a different phase delay of the TAG lens, corresponding to different z -positions. An experimental calibration of the relation between pulse delay and z -positions is derived by performing sharpness tests on the series of images taken at different phase delays and is shown in Fig. 4b. The sharpness of the images is determined using prior approaches in the literature based on filtering the 2D Fourier transform frequency spectra (Zhang et al. 1999; De and Masilamani 2013). The normalized magnification of the captured images versus the focal position z is shown in Fig. 4c, demonstrating a nearly constant magnification across all focal positions. Thus, we demonstrate a high-speed 3D wide-field microscopy technique that can capture volumetric information over a field of size 2.5 mm in width and $600 \mu\text{m}$ in depth with a theoretical temporal resolution $1/70 \text{ kHz} \approx 14.2 \mu\text{s}$. Due to the limitations of our high-speed camera, our experimental setup has a temporal resolution of 1.2 ms. However, anticipating the future availability of high-speed cameras, our setup serves as a proof of concept for higher temporal resolution 3D imaging systems.

3.2 Tracking two particles at different depths

We now apply this microscopy technique to a simple unidirectional flow, and track the motion of two particles at

Fig. 4 **a** Sharpest images of the resolution target taken at different z -positions. The uniformity across the three images demonstrates the nearly constant magnification achieved by the afocal system. The scale bar shown is $100 \mu\text{m}$. **b** Calibration curve between the phase delay and experimental z -position of the resolution target. **c** Normalized magnifications of the resolution target at different z -positions



different z -positions in the depth direction. For this test case, the flow is in the inlet section of the arrow-shaped junction (Fig. 3). In this region of the geometry, the flow is nearly parallel, and so the particles in the flow experience no motion in the z -direction. Because of constraints in our high-speed camera's acquisition rate, we set the system to record six images every time the TAG lens scans through the channel. Thus, for every oscillation cycle of the lens, we capture images at six different focal positions in the depth direction. To determine the z -position of each particle, we first calculate the sharpness of a particle in each of the captured image planes. The z -position of that particle is then ascribed to the plane with the maximum sharpness. The spatial resolution in the x - y plane is $7.4 \mu\text{m}$ and the spacing between z -planes is $50 \mu\text{m}$. In Fig. 5, we demonstrate this procedure on two moving particles. The flow is in the positive y -direction. The left column of the figure shows the consecutive images that were captured at the $z = -100 \mu\text{m}$ focal plane, and the right column shows the consecutive images that were captured at the $z = +300 \mu\text{m}$ focal plane.

3.3 Tracking many particles in flow systems

We track many particles to construct a flow field in a straight-square channel. The fluid flows at a Reynolds number of $Re = 1$. For this case, we perform three sets of experiments with 6 planes each, giving a total of $18 \times 50 \mu\text{m}$ planes throughout the domain. This was done to allow us to capture data over a larger z range of almost the entire 1 mm channel. Alternately, with a faster high-speed camera, this data could have been captured in a single experiment. The captured velocity data are compared with the theoretical predictions in Fig. 6. With zero error, the color of the data points would match the corresponding color of

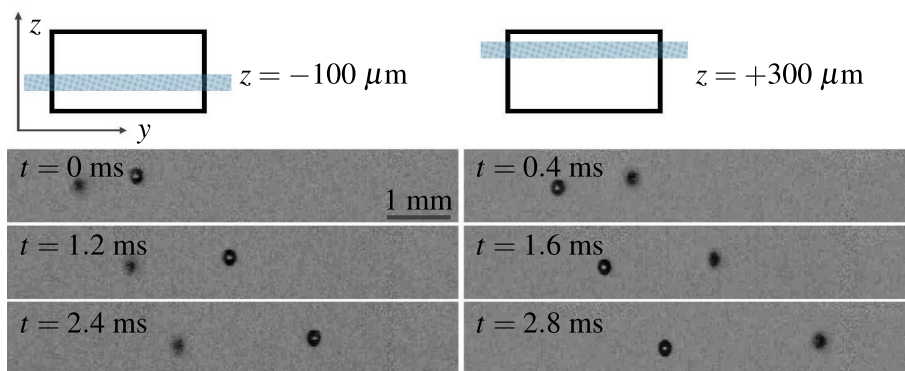


Fig. 5 Simultaneous tracking of two beads at different depth positions z . Time evolves from *left to right* and *top to bottom*. The flow is from *left to right* (positive y -direction). The images on the *left* correspond to the particle that is located at $z = 100 \mu\text{m} \pm 25 \mu\text{m}$, and

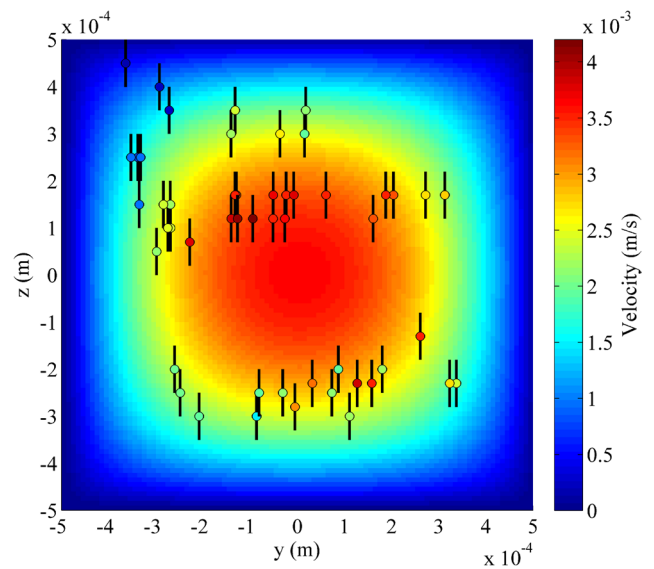


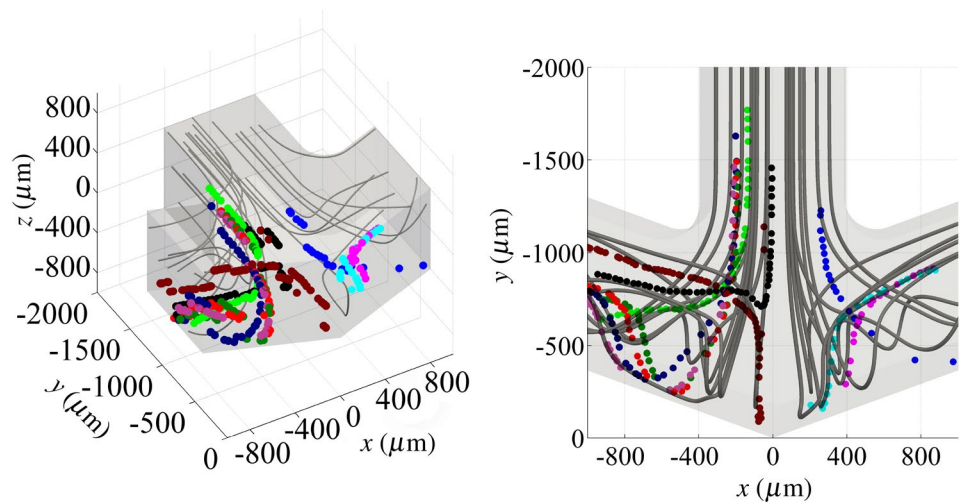
Fig. 6 Experimental velocity profile in a straight, square channel is shown with the theoretical velocity values presented in the background $Re = 1$

the background (theoretical) colormap. The system may suffer from bias caused by the imaging process and tracking methods. These errors can be quantified by the relative mean velocity error and relative mean absolute velocity error, which are 4.3% and 23.5%, respectively.

Now, we apply this microscopy technique to the complex swirling flow located in the junction shown in Fig. 3. As before, we utilize six focal planes. With this particle velocimetry technique, there is a trade-off between the total depth of field in the z -direction, the spatial resolution in the depth direction, and the temporal resolution. Assuming a desired depth of field Δz , and a desired number of focal planes N , the achieved spatial resolution in the depth

the images on the right correspond to the particle that is located at $z = +300 \mu\text{m} \pm 25 \mu\text{m}$. Here, the time step between successive images of the same particle is 1.2 ms, and the time between images of the *lower and upper particles* is 0.4 ms

Fig. 7 Experimental particle tracking data plotted along with several streamlines to show the expected motion of the flow $Re = 160$. As can be seen, the particle motions behave reasonably as expected, demonstrating that this technique is capable of simultaneously tracking multiple particles in flows with complex 3D features. Here, the average inlet velocity is $U_{\text{avg}} = 0.206$ m/s. Each set of colored dots represents the path of one particle. The time step between successive particle captures is $\Delta t = 0.2$ ms



direction will be $\Delta z/N$. Then, for a desired temporal resolution (time step) Δt , the high-speed camera must be able to achieve a frame rate of $N/\Delta t$. Since the TAG lens has the ability to scan in the kHz to MHz range, the ability to achieve high temporal resolution and spatial resolution in the depth direction is limited by the state of the art in high-speed camera technology. However, anticipating future advances in the performance and availability of high-speed cameras, the use of only several focal planes is sufficient here as a proof of concept.

Experimental results using this technique to track multiple particles are shown in Fig. 7. Here, because of the limitation of camera rate, we capture six focal planes in a smaller scanning range, $z = -400 \mu\text{m}$ to $z = -150 \mu\text{m}$, where each plane is separated by $50 \mu\text{m}$. The period of oscillation for the volumetric imaging is 1.2 ms, and the typical magnitude of velocity in the flow is $U_{\text{avg}} = 0.206$ m/s. As can be seen in Fig. 7, the observed 3D particle trajectories behave similarly with the simulated streamlines of the flow. With the limited frame rate of our high-speed camera, to more accurately resolve the 3D flow features, a smaller depth of field may be used, centered around the features of interest. A larger number of focal planes may be utilized, at the expense of temporal resolution. Ultimately, a faster high-speed camera will enable this technique to be used with high temporal and spatial accuracy to visualize complex, 3D flows.

4 Conclusion

We have demonstrated a fast axial-scanning wide-field microscopy technique for volumetric particle tracking velocimetry by integrating a TAG lens, scanning at a frequency of 70 kHz, with a wide-field microscope to acquire images through the scanning volume every $7.14 \mu\text{s}$. The

ability to quickly and precisely visualize complex 3D flow fields and particle dynamics is essential for understanding flow structures and natural dynamics in many complex systems. We achieve this result by synchronizing a TAG lens with a pulsed LED and camera shutter to capture images at different z -positions within the scanning cycle of the lens. We eliminate the variation in image magnification by aligning the principal plane of the TAG lens with the aperture stop of the objective, which is critical for imaging accuracy. Therefore, the single-camera imaging system proposed in the paper provides a simple and economical means of high-speed three-dimensional visualization.

With this high-speed 3D imaging technique, we were able to simultaneously capture multiple particle trajectories in the complex vortical flow within an arrow-shaped junction with a time resolution of sub-milliseconds. We emphasize that the temporal and spatial resolutions of this technique are limited only by the image acquisition rate of the available camera (based upon the needs of the experiment of interest). With an upper bound on the TAG lens oscillation frequency in the MHz range, sub-microsecond volumetric particle tracking velocimetry measurements are theoretically possible with this technique.

Acknowledgements The authors thank TAG Optics Inc., David Amrhein, and Christian Therlault for technical support, and gratefully acknowledge financial support from the NSF (Grant No. CMMI-1235291) and the Ministry of Education, Republic of China. T-H. Chen thanks Marcus Hultmark and Romain Fardel for useful discussions.

References

- Ault JT, Fani A, Chen KK, Shin S, Gallaire F, Stone HA (2016) Vortex-breakdown-induced particle capture in branching junctions. *Phys Rev Lett* 117(8):084501

- Chen BC, Legant WR, Wang K, Shao L, Milkie DE, Davidson MW, Janetopoulos C, Wu XS, Hammer JA, Liu Z, English BP, Mimori-Kiyosue Y, Romero DP, Ritter AT, Lippincott-Schwartz J, Fritz-Laylin L, Mullins RD, Mitchell DM, Bembenek JN, Reymann AC, Bohme R, Grill SW, Wang JT, Seydoux G, Tulu US, Kiehart DP, Betzig E (2014) Lattice light-sheet microscopy: imaging molecules to embryos at high spatiotemporal resolution. *Science* 346(6208):1257–998. doi:[10.1126/science.1257998](https://doi.org/10.1126/science.1257998)
- Chen KK, Rowley CW, Stone HA (2015) Vortex dynamics in a pipe T-junction: recirculation and sensitivity. *Phys Fluids* 27:034107
- Choi YS, Lee SJ (2009) Three-dimensional volumetric measurement of red blood cell motion using digital holographic microscopy. *Appl Opt* 48(16):2983. doi:[10.1364/ao.48.002983](https://doi.org/10.1364/ao.48.002983)
- Cierpka C, Kähler CJ (2011) Particle imaging techniques for volumetric three-component (3d3c) velocity measurements in microfluidics. *J Vis* 15(1):1–31. doi:[10.1007/s12650-011-0107-9](https://doi.org/10.1007/s12650-011-0107-9)
- De K, Masilamani V (2013) Image sharpness measure for blurred images in frequency domain. *Proc Eng* 64:149–158
- Dennis DJC, Nickels TB (2011) Experimental measurement of large-scale three-dimensional structures in a turbulent boundary layer. part 2. long structures. *J Fluid Mech* 673:218–244. doi:[10.1017/s0022112010006336](https://doi.org/10.1017/s0022112010006336)
- Duocastella M, Sun B, Arnold CB (2012) Simultaneous imaging of multiple focal planes for three-dimensional microscopy using ultra-high-speed adaptive optics. *J Biomed Opt* 17(5):050,505. doi:[10.1117/1.jbo.17.5.050505](https://doi.org/10.1117/1.jbo.17.5.050505)
- Duocastella M, Vicidomini G, Diaspro A (2014) Simultaneous multiplane confocal microscopy using acoustic tunable lenses. *Opt Express* 22(16):19,293. doi:[10.1364/oe.22.019293](https://doi.org/10.1364/oe.22.019293)
- Elsinga GE, Scarano F, Wieneke B, van Oudheusden BW (2006) Tomographic particle image velocimetry. *Exp Fluids* 41(6):933–947. doi:[10.1007/s00348-006-0212-z](https://doi.org/10.1007/s00348-006-0212-z)
- Grothe RL, Dabiri D (2008) An improved three-dimensional characterization of defocusing digital particle image velocimetry (DDPIV) based on a new imaging volume definition. *Meas Sci Technol* 19(6):065,402. doi:[10.1088/0957-0233/19/6/065402](https://doi.org/10.1088/0957-0233/19/6/065402)
- Klein SA, Moran JL, Frakes DH, Posner JD (2012) Three-dimensional three-component particle velocimetry for microscale flows using volumetric scanning. *Meas Sci Technol* 23(8):085,304. doi:[10.1088/0957-0233/23/8/085304](https://doi.org/10.1088/0957-0233/23/8/085304)
- McLeod E, Arnold CB (2007) Mechanics and refractive power optimization of tunable acoustic gradient lenses. *J Appl Phys* 102(3):033,104. doi:[10.1063/1.2763947](https://doi.org/10.1063/1.2763947)
- Mermillod-Blondin A, McLeod E, Arnold CB (2008) High-speed varifocal imaging with a tunable acoustic gradient index of refraction lens. *Opt Lett* 33(18):2146. doi:[10.1364/ol.33.002146](https://doi.org/10.1364/ol.33.002146)
- Olivier N, Mermillod-Blondin A, Arnold CB, Beurepaire E (2009) Two-photon microscopy with simultaneous standard and extended depth of field using a tunable acoustic gradient-index lens. *Opt Lett* 34(11):1684. doi:[10.1364/ol.34.001684](https://doi.org/10.1364/ol.34.001684)
- Park JS, Choi CK, Kihm KD (2004) Optically sliced micro-PIV using confocal laser scanning microscopy (CLSM). *Exp Fluids* 37(1):105–119. doi:[10.1007/s00348-004-0790-6](https://doi.org/10.1007/s00348-004-0790-6)
- Park JS, Kihm KD (2005) Three-dimensional micro-PTV using deconvolution microscopy. *Exp Fluids* 40(3):491–499. doi:[10.1007/s00348-005-0090-9](https://doi.org/10.1007/s00348-005-0090-9)
- Pereira F, Gharib M (2002) Defocusing digital particle image velocimetry and the three-dimensional characterization of two-phase flows. *Meas Sci Technol* 13(5):683–694. doi:[10.1088/0957-0233/13/5/305](https://doi.org/10.1088/0957-0233/13/5/305)
- Prasad AK (2000) Stereoscopic particle image velocimetry. *Exp Fluids* 29(2):103–116. doi:[10.1007/s003480000143](https://doi.org/10.1007/s003480000143)
- Vettenburg T, Dalgarno HIC, Nylk J, Coll-Lladó C, Ferrier DEK, Čížmár T, Gunn-Moore FJ, Dholakia K (2014) Light-sheet microscopy using an airy beam. *Nature Methods* 11(5):541–544. doi:[10.1038/nmeth.2922](https://doi.org/10.1038/nmeth.2922)
- Vigolo D, Griffiths IM, Radl S, Stone HA (2013) An experimental and theoretical investigation of particle-wall impacts in a T-junction. *J Fluid Mech* 727:236–255. doi:[10.1017/jfm.2013.200](https://doi.org/10.1017/jfm.2013.200)
- Vigolo D, Radl S, Stone HA (2014) Unexpected trapping of particles at a T-junction. *Proc Natl Acad Sci* 111(13):4770–4775. doi:[10.1073/pnas.1321585111](https://doi.org/10.1073/pnas.1321585111)
- Wereley ST, Meinhart CD (2010) Recent advances in micro-particle image velocimetry. *Annu Rev Fluid Mech* 42(1):557–576. doi:[10.1146/annurev-fluid-121108-145427](https://doi.org/10.1146/annurev-fluid-121108-145427)
- Westerweel J, Elsinga GE, Adrian RJ (2013) Particle image velocimetry for complex and turbulent flows. *Annu Rev Fluid Mech* 45(1):409–436. doi:[10.1146/annurev-fluid-120710-101204](https://doi.org/10.1146/annurev-fluid-120710-101204)
- Willert CE, Gharib M (1992) Three-dimensional particle imaging with a single camera. *Exp Fluids* doi:[10.1007/bf00193880](https://doi.org/10.1007/bf00193880)
- Zhang NF, Postek MT, Larrabee RD, Vldar AE, Keery WJ, Jones SN (1999) Image sharpness measurement in the scanning electron microscope-part III. *Scanning* 21(4):246–252
- Zong W, Zhao J, Chen X, Lin Y, Ren H, Zhang Y, Fan M, Zhou Z, Cheng H, Sun Y, Chen L (2014) Large-field high-resolution two-photon digital scanned light-sheet microscopy. *Cell Res* 25(2):254–257. doi:[10.1038/cr.2014.124](https://doi.org/10.1038/cr.2014.124)